Supplementary Information

Liquid Phase Transmission Electron Microscopy with flow and temperature control

J. Tijn van Omme[1], Hanglong Wu[2], Hongyu Sun[1], Anne France Beker[1], Mathilde Lemang[1], Ronald G. Spruit[1], Sai P. Maddala[2], Alexander Rakowski[3], Heiner Friedrich[2], Joseph P. Patterson[3*], H. Hugo Pérez Garza[1]

[1] *DENSsolutions B.V., Informaticalaan 12, Delft, 2628 ZD, The Netherlands*

[2] *Physical Chemistry, Department of Chemical Engineering and Chemistry and Institute for Complex Molecular Systems, Eindhoven University of Technology, Eindhoven, The Netherlands*

[3] *Department of Chemistry, University of California, Irvine, Irvine CA 92697-2025, United States*

[*] Corresponding author: patters3@uci.edu; tel. +1 949-529-6854.

S1 Challenges for LPTEM

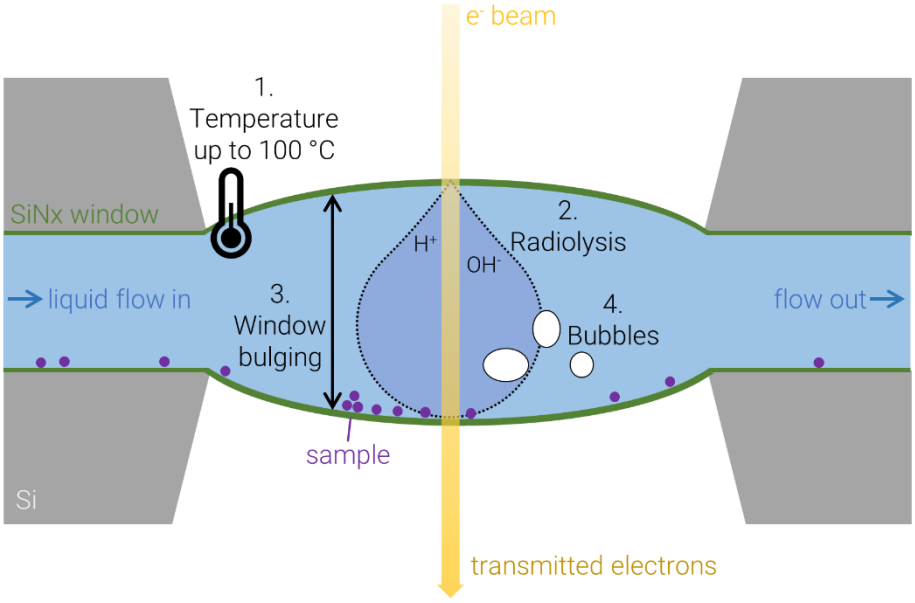

Supplementary Figure S1 Schematic showing the typical challenges for LPTEM experiments at elevated temperature (not to scale).

1. *Accurate and homogeneous temperature*. It is not always trivial to know the temperature of the sample and the liquid in the viewable area.[1] When the heating is done externally or using the furnace-type holder, the temperature is not measured close to the sample, and temperature gradients may arise in the sample area. MEMS-based heating chips are more suitable for this, as they rely on a heating spiral close to the sample that acts as both the heater as well as the temperature sensor. Typically, a resistive heating coil is used of which the material has a well-defined temperature dependent resistance. MEMS-based heaters additionally feature lower drift than other types of holders, as they require less power to heat up.[2]
2. *Electron-beam influence*. In any liquid cell experiment, the effect of the electron beam must always be taken into account.[3,4] Not only the electron flux (e^-/nm^2s), but also the total electron irradiation (e^-/nm^2) was found to have a large effect, most commonly because of radiolysis.[5,6] Even greater care is required if the event of interest can be triggered both by a temperature increase as well as by the high energy electrons in the beam, for example a nucleation event. The heating effect and the e-beam effect must be separated by careful control experiments.
3. *Thickness of the liquid layer*. Both in TEM mode and Scanning TEM (STEM) mode, the achievable resolution is mainly determined by the thickness of the liquid layer.[7,8] In thinner layers, the broadening of the electron beam is minimized, resulting in higher resolution and better contrast. But the liquid may also not be too thin, otherwise it loses its bulk-like properties.[9,10]

   The liquid thickness is the summation of the distance between the two chips and the window bulging, which arises from the pressure difference across the windows. When performing experiments at elevated temperature, the components of the system will experience thermal expansion. Apart from the bothersome sample drift[1], this will lead to an increase in both of these factors determining liquid layer thickness. This

makes it difficult for experiments at elevated temperature to achieve high resolution.

4. *Bubbles.* Finally, a commonly encountered problem is the formation of a gas bubble in the viewable area.[3,7,11] Sometimes this can be used as an advantage, for example to perform high resolution imaging without the liquid present. However, normally the interest lies in *in situ* imaging in liquid, such that a dry viewable area is not desirable. Compared to an experiment at room temperature, heating will make this problem more severe. Bubbles are more likely to form as the gas dissolved into the liquid becomes less soluble because of the higher temperature. In other words, the liquid reaches a higher level of supersaturation of the gas that is dissolved into it and tends to start forming bubbles.[12] Moreover, once formed, the bulging of the membranes allows the bubble to reach a shape close to spherical. This makes the bubble stick to the viewable area.[13]

S2 Complete Stream Liquid Heating system

To complete the Stream Liquid Heating system, the MEMS devices that form the Nano-Cell are assembled in their dedicated *in situ* holder. This functionalized sample holder incorporates the inlet and outlet tubing, as well as the electrical feedthroughs to apply the voltage to the heater (Supplementary Figure S2a). Outside of the TEM, the tubing is connected to inlet and outlet reservoirs, on which the desired pressure is applied by the pressure-based pump. A laptop allows the user to simultaneously control these pressures, as well as the temperature of the microheater. Note that apart from the holder, no specialized TEM setup is required, therefore this system represents a cost-effective supplement for the TEM.

Typically, the workflow consists of several steps before inserting the holder into the TEM. First, if required, a sample is deposited on one of the chips, after which the bottom chip is placed in the tip of the holder. The top chip with the O-ring in its groove is placed on top and the stack is compressed by tightening the screws of the lid at a low torque. With the dedicated alignment tool, shown in Supplementary Figure S2b-c, the top window can be moved with respect to the bottom. A digital microscope camera allows the user to observe if the windows are overlapping and, if necessary, to make sure a FIB lamella, localized drop cast or other area of interest, ends up in the viewable area in the TEM. The screws are then tightened to their final torque to create a leak tight seal that closes the Nano-Cell. A leak test is performed in the leak test station (Supplementary Figure S2f) to confirm that all connections are sealing properly, such that the holder can be inserted into the TEM.

Following a modular design approach, the holder can be disassembled completely, as shown in Supplementary Figure S2d. All the components that come into contact with the liquid can be taken apart to be cleaned, for example in an ultrasonic bath with ethanol. This way, clogging and/or cross contamination between experiments is avoided. An additional benefit of this modular design is the possibility to exchange components depending on their chemical compatibility, especially the O-rings and the tubing material. Polyether ether ketone (PEEK) was selected as the most appropriate general-purpose material for the tubing inside and outside of the holder, due to its chemical robustness that is maintained also at high temperature. A wide range of pH conditions can be used without attacking the material.

Finally, the holder is optimized for EDS analysis, such that chemical analysis of the sample and reaction products can be done. The holder must be tilted towards the EDS detector (side entry or Super-X) to prevent shadowing of the detector. The high tilt (+/- 30 °) and the lid design make sure that the number of counts per second is maximized. In the top chip, the window orientation is chosen such that the sample faces the EDS detector, and additional material is removed to further reduce shadowing, see Supplementary Figure S2e.

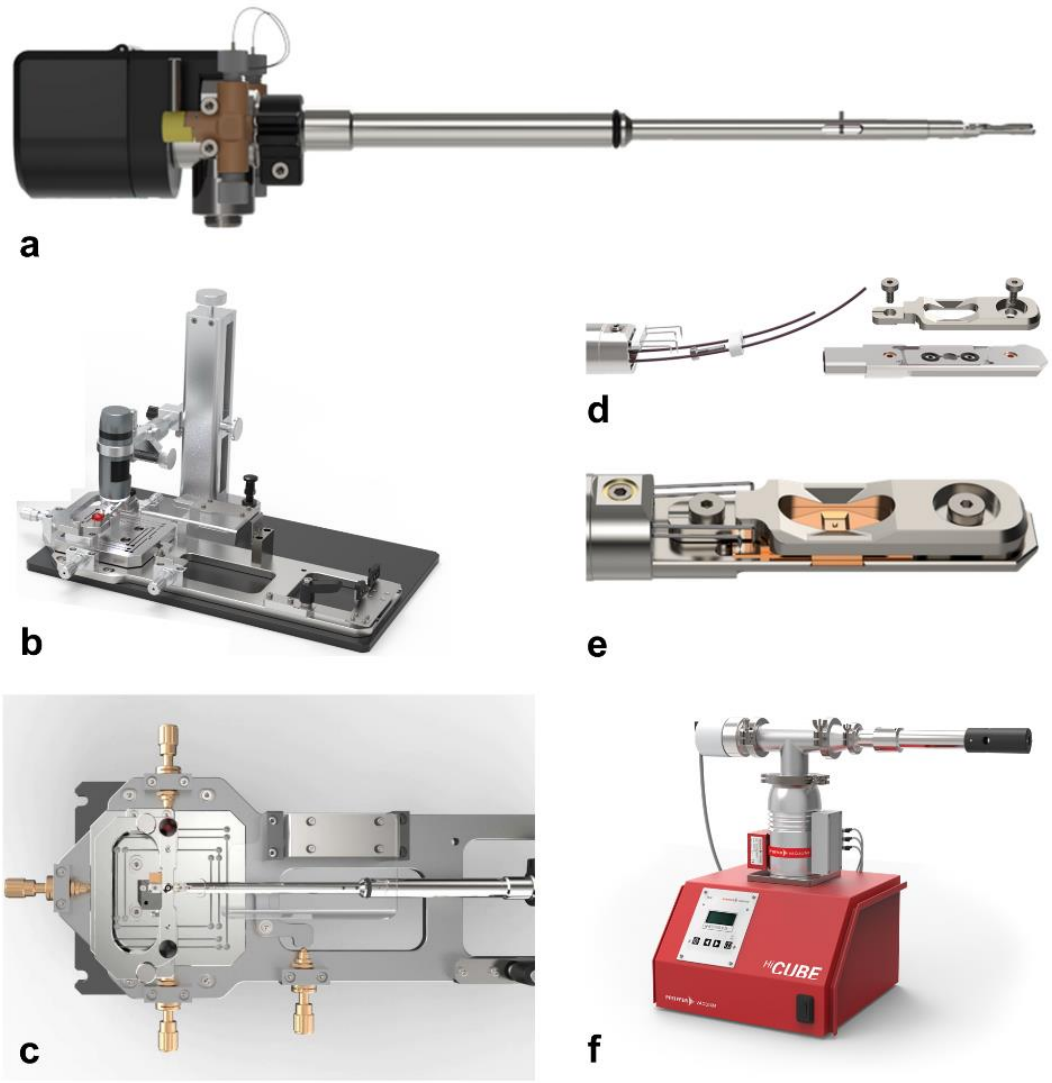

Supplementary Figure S2 Stream Liquid Heating holder and tooling. (**a**) Assembled holder. The tubing from and to the liquid reservoirs is connected to the valves on the back of the holder. (**b**) Alignment station with digital microscope. (**c**) Top view of the alignment station and holder showing the micrometer screws that are used to move the lid with the top chip to the desired position. (**d**) The modular holder tip can be disassembled for cleaning. (**e**) Holder tip with assembled Nano-Cell. Lid and top chip have indentations to optimize EDS detection. (**f**) Leak test station.

S3 Using pressure control to remove a bubble

An assembled Nano-Cell was inserted into the TEM and filled with ultrapure water (inlet pressure 2000 mbar, outlet pressure 200 mbar). A gas bubble was nucleated using the electron beam at high dose for a short time. In order to create a situation of undersaturation and dissolve the bubble, the Nano-Cell pressure was increased from 1100 mbar to 1500 mbar (inlet pressure kept at 2000 mbar, outlet pressure increased to 1000 mbar).

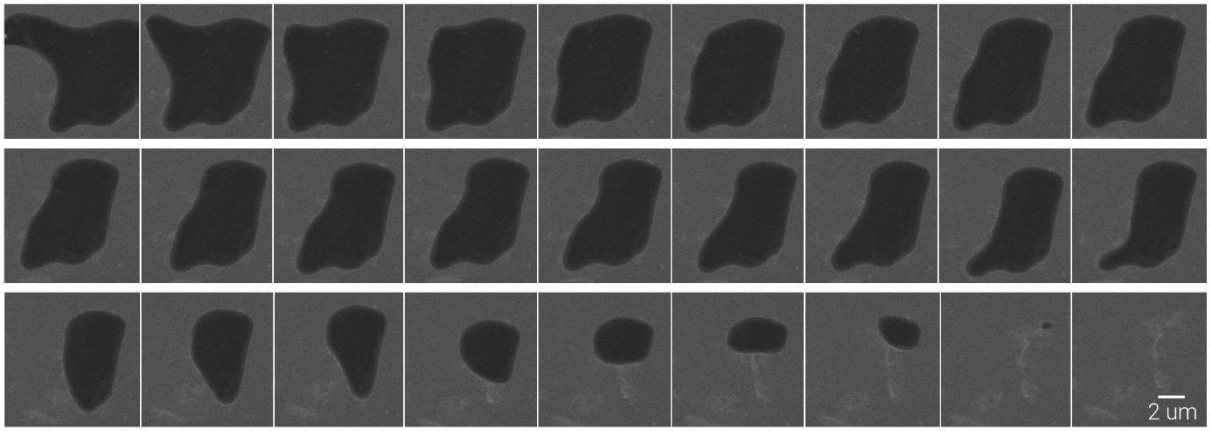

Supplementary Figure S3 Dissolution of a purposely introduced bubble. Each frame is 0.33 seconds (total time 8.6 s)

S4 Sample preparation: Synthesis and deposition of silica nanoparticles

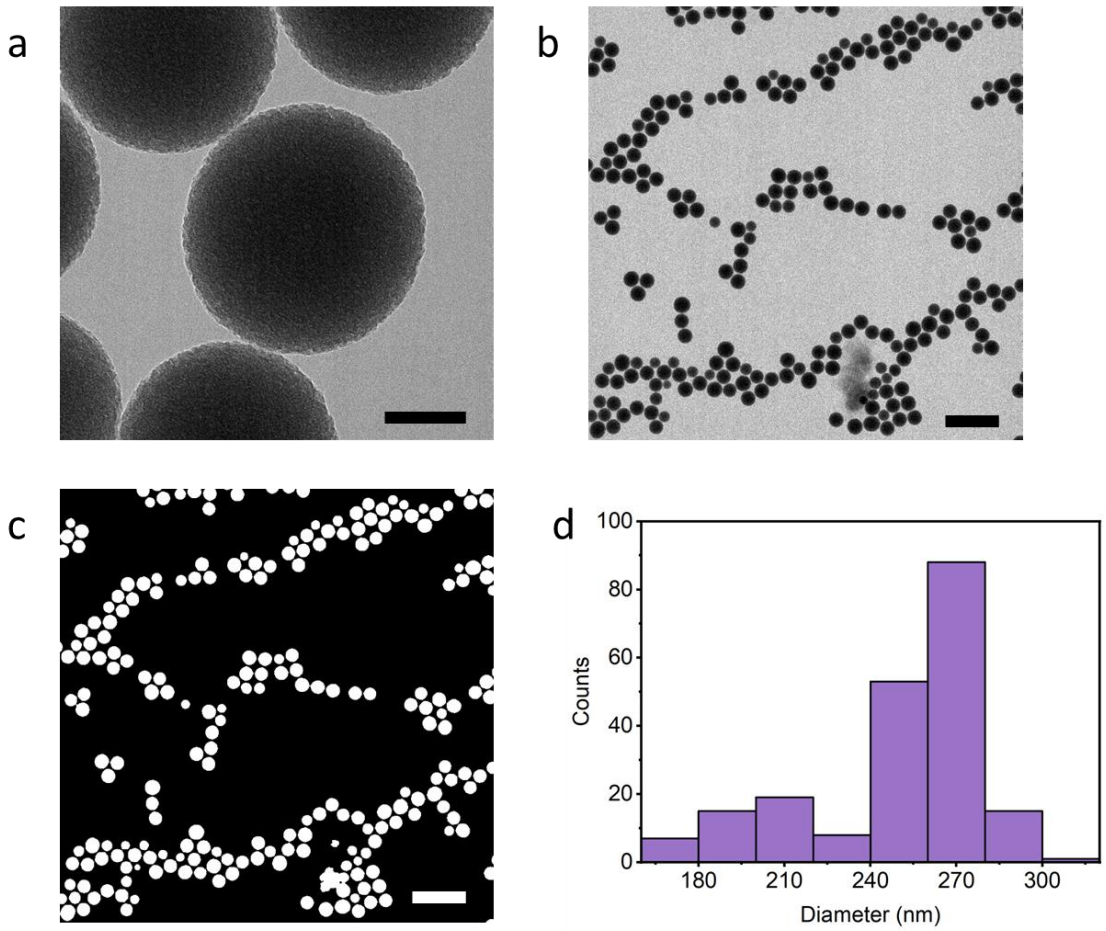

Supplementary Figure S4.1 Dry TEM of the as-prepared silica nanoparticles. (**a-b**) High and low magnification TEM images of silica nanoparticles. Scale bars in (a) and (b) are 100 nm and 1 µm, respectively. (**c**) Binary image processed from (b) using Otsu method for particle area and diameter measurements.[14] Note that only spherical particles were used for statistical analysis. Scale bar, 1 µm. (**d**) Particle size distribution of silica nanoparticles calculated from (c), where 206 particles were measured.

a

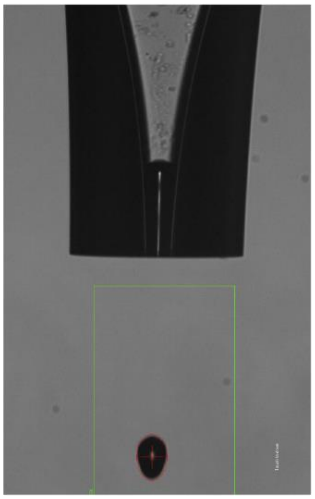

b

	20 °C	40 °C	60 °C
Volume of sinlge droplet (pL)	349.76	301.03	295.22
Number of droplets loaded	3	2	2

c

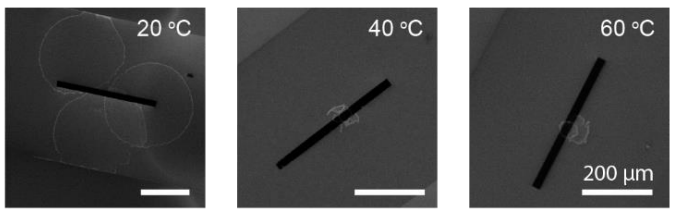

Supplementary Figure S4.2 Ultra-low volume liquid dispenser sciTEM assists the sample loading for the liquid heating experiments. (**a**) A well-defined droplet being dispensed by sciTEM. The nozzle can shoot ca. 200 droplets

in 1 second. (**b**) Overview of the volume of droplets dispensed on the chips for 20 °C, 40 °C and 60 °C experiments. (**c**) SEM images of the coffee-rings resulting from sample droplets on chips for different temperature experiments. The coffee-rings are in the center of the window area of the bottom chip.

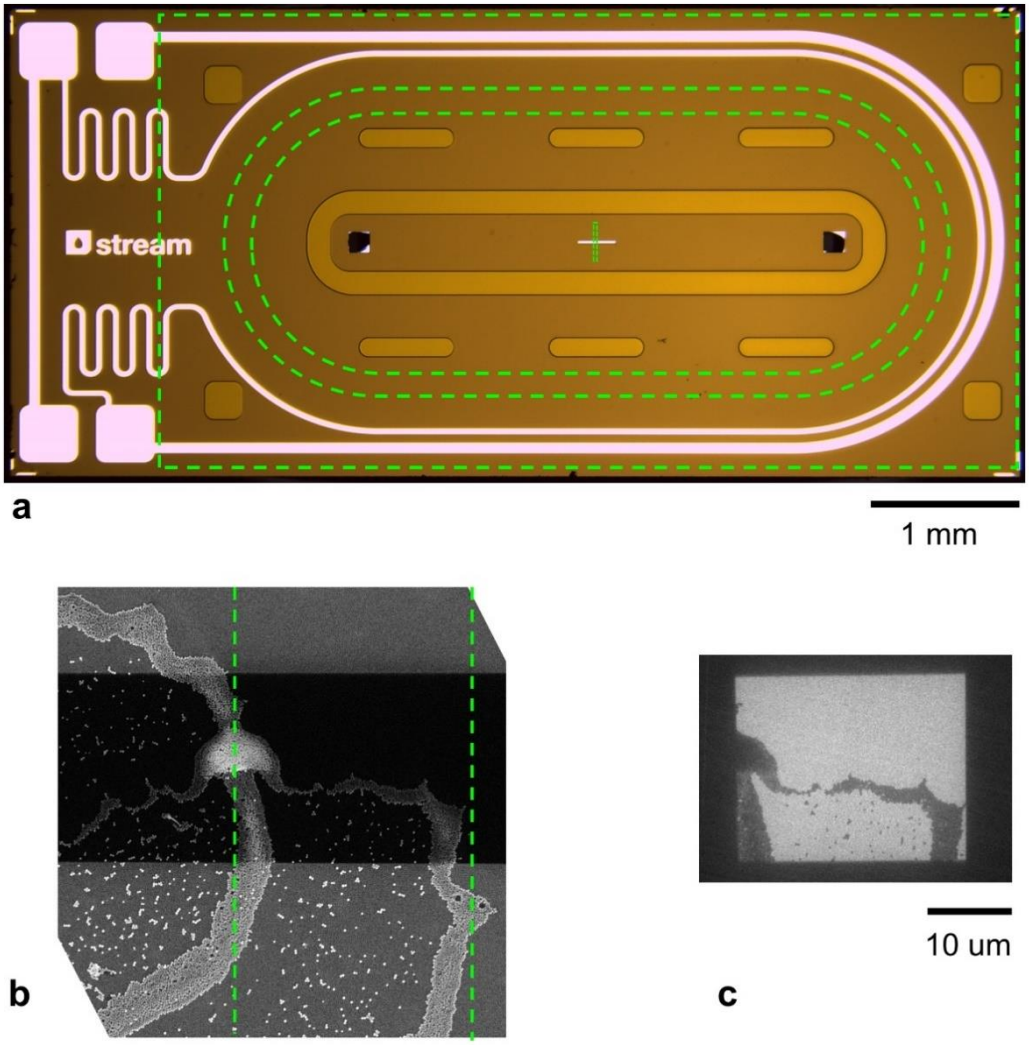

Supplementary Figure S4.3 Window alignment (**a**) Optical microscopy image of the Stream bottom chip after microfabrication. Dotted lines represent the position of the top chip with its O-ring groove and the top window perpendicular to the bottom window. (**b**) SEM image of the deposited silica nanoparticles for the 60 °C etching experiment, after the localized droplet placement. The dedicated alignment tool was used to align the top window across the area of interest. Dotted lines show how the top window was aligned. (**c**) Low magnification TEM image showing the overview of the viewable area.

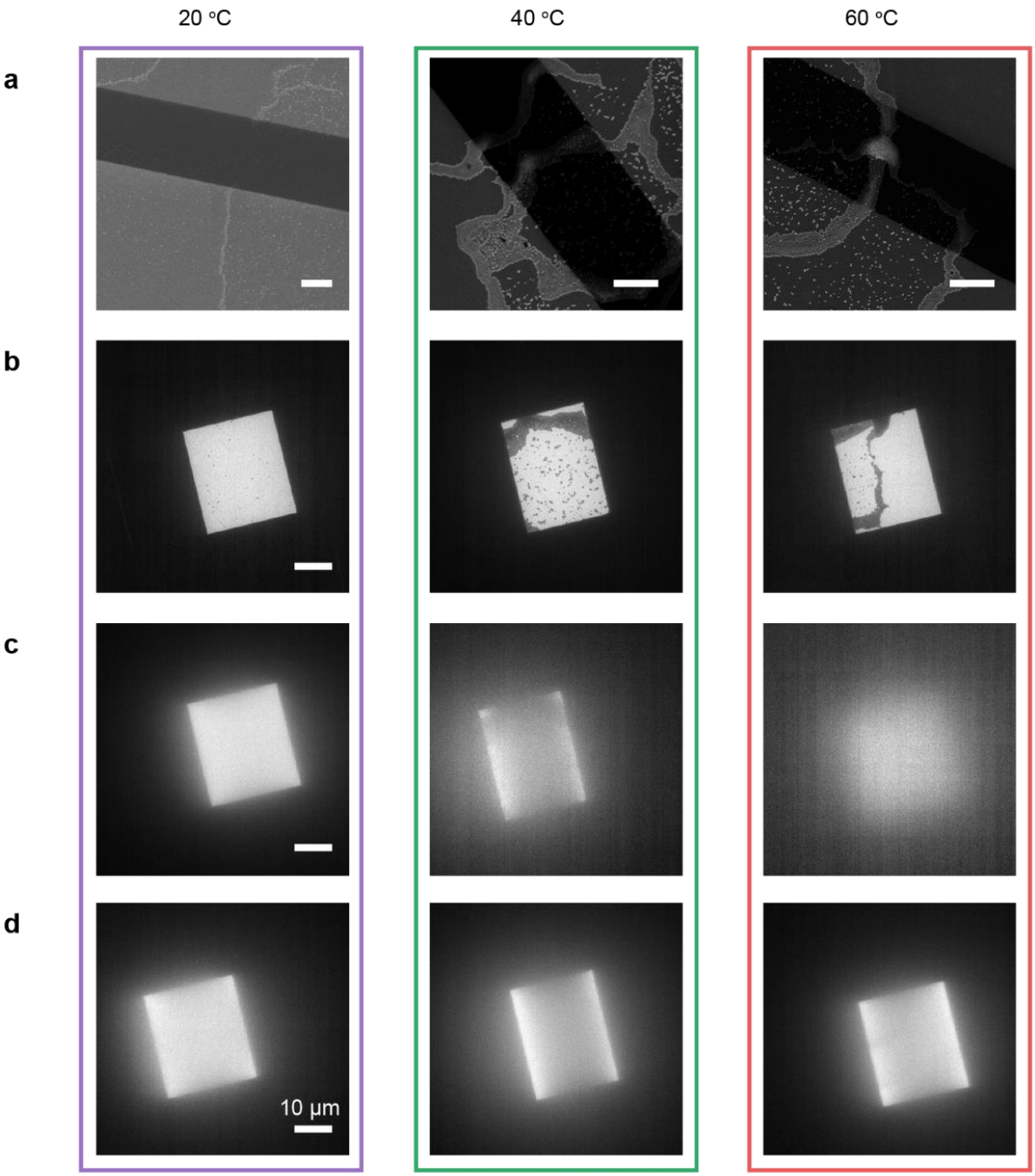

Supplementary Figure S4.4: Overview of the window area of the liquid cell before and after imaging at different temperatures. (**a**) SEM images of the center window area of the bottom chip before cell assembly. (**b**) Low-mag TEM images of window area of the assembled cells for different temperature LPTEM experiments before flowing NaOH. (**c**) Low-mag TEM images of window area of the liquid cells right after being filled with NaOH. (**d**) Low-magnification TEM images of window area of the liquid cells after the etching experiments are finished, indicating the cells are still hydrated.

S5 Data analysis

The data analysis was performed by in house scripts programmed in MATLAB (Mathworks), including several stages: (1) Alignment of the image stack; (2) Determination of relative intensity; (3) Relative intensity changes vs time.

1. Alignment of the image stack

Due to the acquisition protocol and the stage drift, when individual frames were converted into the image stack, significant sample drift was observed, which prevents direct quantitative analysis. To alleviate the problem, the shift between frames was estimated using a normalized two-dimensional cross-correlation (N2DCC). The following general procedure is employed:

(1) Crop out an area containing the targeted feature; (2) Calculate N2DCC between the template and each frame; (3) find the peak location in the cross-correlation in each frame; (4) calculate the shift of the peak in each frame; (5) Apply the shift to each frame to correct the drift between subsequent frames.

After drift correction, regions of interests (ROI) were cropped out. (Supplementary Movie 3 and Figures S5.1-2). In order to perform single particle quantitative analysis, we also cropped and stabilized the areas only containing a single silica nanoparticle (Supplementary Movie 4 and Figure S5.1-2).

2. Determination of relative intensity

To correct the background variation over different frames and to better compare the etching dynamics among different silica nanoparticles, the relative intensity was employed in displaying images instead of the raw data using an in-house MATLAB code. For the single frame i in the aligned stack,

$$Relative\ intensity_i = \frac{I_i}{\bar{I}_{bg,i}}$$

Where I_i is the original intensity of the image, and $\bar{I}_{bg,i}$ is the mean intensity of the background area (normally 20 x 20 pixels) in the image.

3. Relative intensity changes vs time

The changes in relative intensity vs time were determined using in-house MATLAB scripts. After the nanoparticle was stabilized, the mean relative intensity of the central area (e.g. 10 ×10 pixels) was calculated from the frames with relative intensity. Assuming that the silica nanoparticle was completely dissolved at the end of the movie, the calculated mean intensities were normalized by the maximum intensity (Figure 5c).

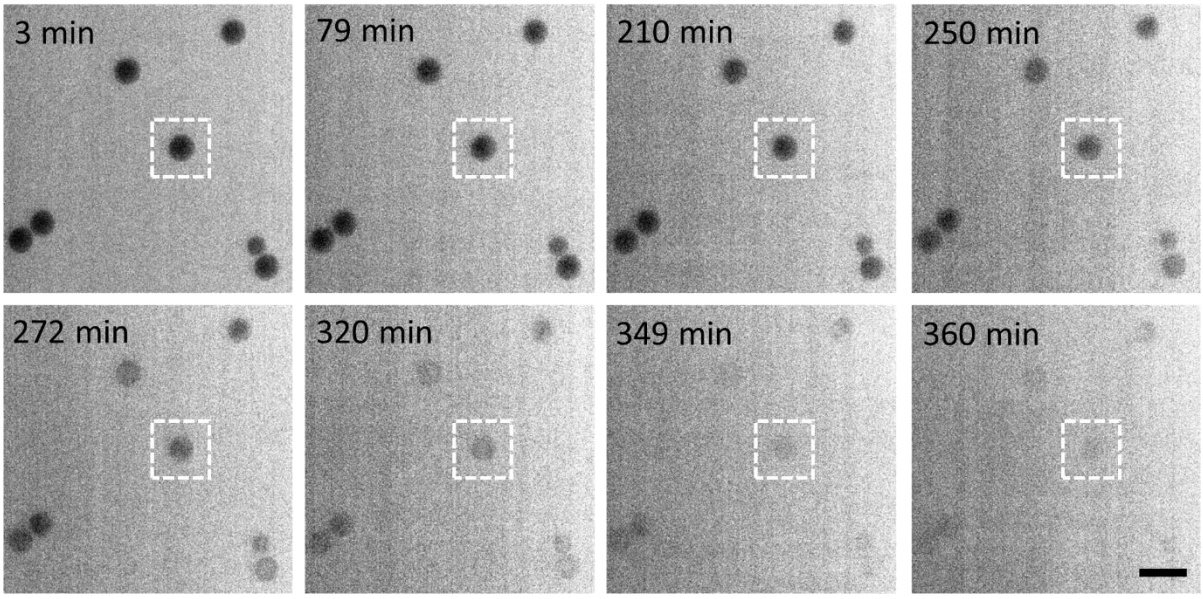

Supplementary Figure S5.1 LPTEM of the silica nanoparticle etching process at 20 °C. The particle in the dashed square box is cropped out to show in Figure 4c of the main text. Scale bar: 500 nm.

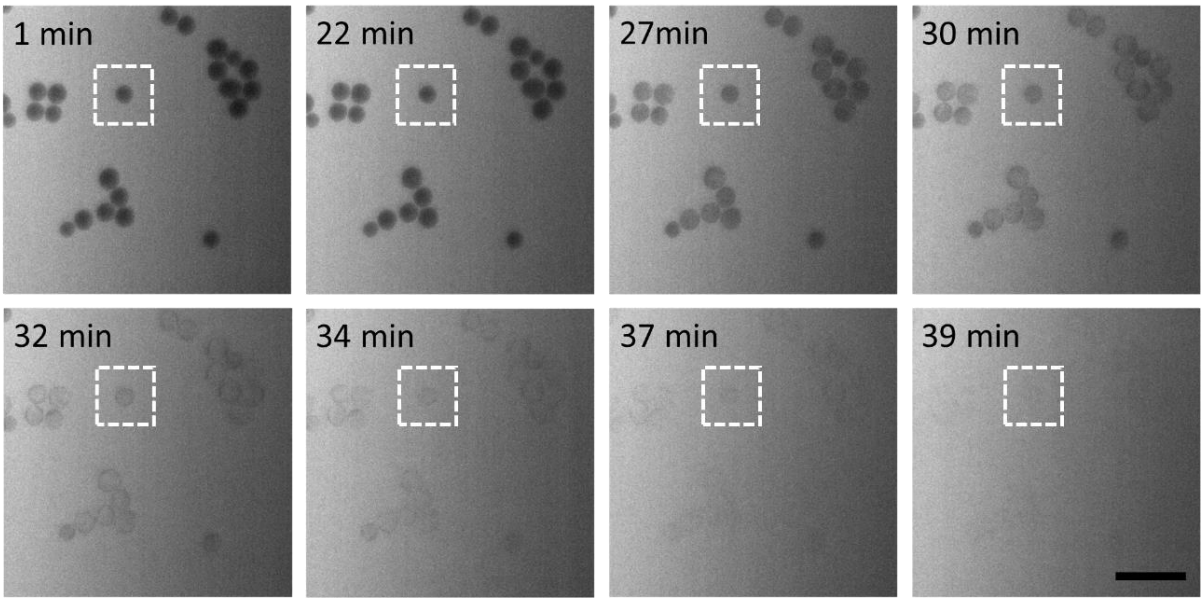

Supplementary Figure S5.2 LPTEM of the silica nanoparticle etching process at 40 °C. The particle in the dashed square box has been cropped out to show in Figure 4c of the main text. Scale bar: 1 µm.

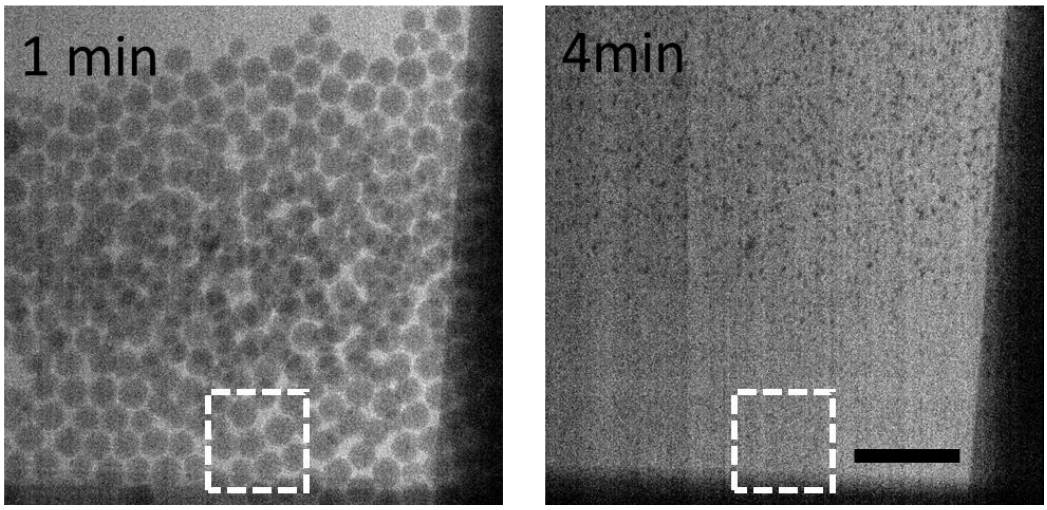

Supplementary Figure S5.3 LPTEM of the silica nanoparticle etching process at 60 °C. The area in the dashed square box has been cropped out to show in Figure 4c of the main text. Scale bar: 1 µm.

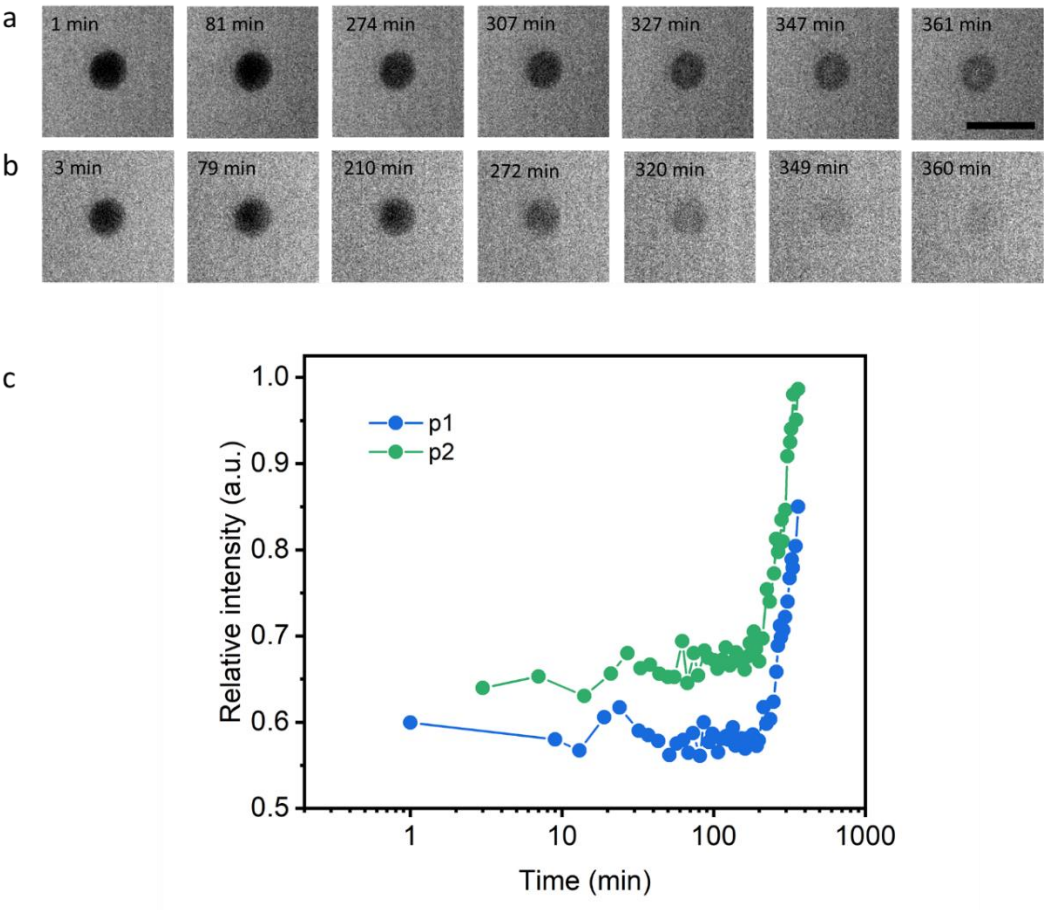

Supplementary Figure S5.4 Comparison of the etching dynamics of two particles from different locations in the same LPTEM experiment. (**a-b**) Snapshots of the etching process, where the particle in (a) is etched more slowly than the particle in (b). (**c**) Evolution of the relative intensity of the two particles with time. Each data point represents 64 pixels averaged in the center of the particle. Temperature: 20 °C. Scale bar: 500 nm.

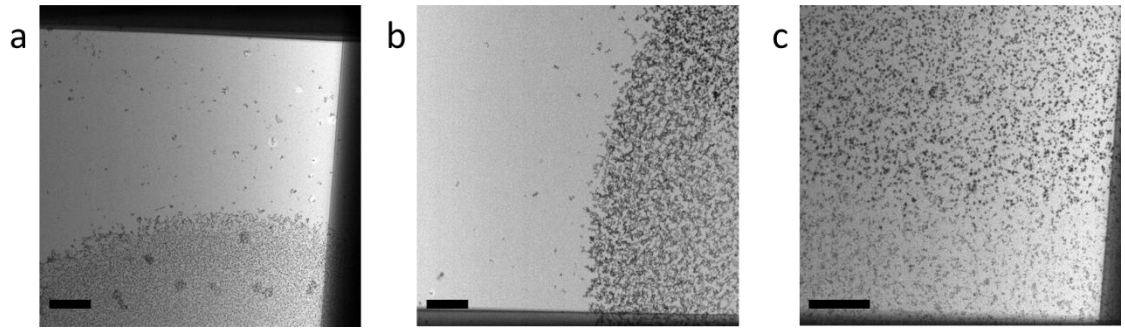

Supplementary Figure S5.5 Electron beam induced particle deposition during 60 °C etching experiments. Scale bars: 1 µm.

REFERENCES

1 M. L. Taheri, E. A. Stach, I. Arslan, P. A. Crozier, B. C. Kabius, T. LaGrange, A. M. Minor, S. Takeda, M. Tanase, J. B. Wagner and R. Sharma, *Ultramicroscopy*, 2016, **170**, 86–95.

2 R. G. Spruit, J. T. van Omme, M. K. Ghatkesar and H. H. Pérez Garza, *J. Microelectromechanical Syst.*, 2017, **26**, 1165–1182.

3 T. J. Woehl, K. L. Jungjohann, J. E. Evans, I. Arslan, W. D. Ristenpart and N. D. Browning, *Ultramicroscopy*, 2013, **127**, 53–63.

4 F. M. Ross, *Science*, 2015, **350**, aaa9886.

5 T. H. Moser, H. Mehta, C. Park, R. T. Kelly, T. Shokuhfar and J. E. Evans, *Sci. Adv.*, 2018, **4**, eaaq1202.

6 T. J. Woehl and P. Abellan, *J. Microsc.*, 2017, **265**, 135–147.

7 K. L. Klein, I. M. Anderson and N. De Jonge, *J. Microsc.*, 2011, **242**, 117–123.

8 N. de Jonge, L. Houben, R. E. Dunin-Borkowski and F. M. Ross, *Nat. Rev. Mater.*, 2019, **4**, 61–78.

9 A. Radisic, P. M. Vereecken, J. B. Hannon, P. C. Searson and F. M. Ross, *Nano Lett.*, 2006, **6**, 238–242.

10 C.-M. Wang, H.-G. Liao and F. M. Ross, *MRS Bull.*, 2015, **40**, 46–52.

11 J. M. Grogan, N. M. Schneider, F. M. Ross and H. H. Bau, *Nano Lett.*, 2014, **14**, 359–364.

12 I. Pereiro, A. Fomitcheva Khartchenko, L. Petrini and G. V. Kaigala, *Lab Chip*, 2019, **19**, 2296–2314.

13 E. R. White, M. Mecklenburg, S. B. Singer, S. Aloni and B. C. Regan, *Appl. Phys. Express*, 2011, **4**, 055201.

14 N. Otsu, *IEEE Trans. Syst. Man. Cybern.*, 1979, **9**, 62–66.